EFFECTS OF PROCESS PARAMETERS ON PHYSICAL AND MECHANICAL PROPERTIES OF FIBER-CEMENT SHEETS

HÜLYA KUS [a], EMIN ÖZGÜR [b], VANDERLEY M. JOHN [c]

[a] ITU Faculty of Architecture, Istanbul, Turkey

[b] Atermit Endüstri Ticaret A.S., Gebze, Turkey

[c] USP Departamento de Engenharia de Construção Civil, Escola Politécnica, São Paulo, Brazil

ABSTRACT

A comparative study is presented in this paper intended for improving knowledge of the effects of process parameters on mechanical and physical properties of fiber-cement corrugated roof sheets. The sheets produced at maximum and minimum values of various process parameters were investigated through bending and layer bonding tests, water absorption, and microstructure analysis using scanning electron microscopy and nitrogen adsorption techniques. The aim of this work is to form a base for conducting an extensive research on this topic with complementary tests and analysis. The study program will be developed based on the preliminary results partly presented in this introductory report.

KEYWORDS:

Fiber cement; flexural strength; layer bonding; water absorption; microstructure; porosity.

INTRODUCTION

Long-term performance and durability of fiber cement composites have been a research concern worldwide, particularly after the replacement of asbestos with natural and synthetic fibers. One of the most important challenges in air cured fiber-cement sheet manufacturing is understanding the difference in mechanical and physical properties of non-asbestos fiber-cement sheets compared to the asbestos ones. Lower modulus of rupture, excessive water absorption, high rates of drying shrinkage which may lead to high porosity, crack formation, delamination, etc. can be regarded as durability issues linked to process parameters.

Characteristics of constituent materials including fibers, matrix and fillers, process agents such as flocculants and anti-foam chemicals, mix proportions, curing conditions, and last but not least, environmental exposure conditions can also be regarded as factors that affect the physical and mechanical properties of the fiber-cement sheets. However the main objective of this study is to gain information on the interrelation between production process parameters and physical and mechanical properties.

Mechanical and physical tests as well as microstructural analysis were included in the research program. So far, flexural strength, layer bonding and water absorption tests were conducted, and nitrogen desorption analysis (porosimetry) and SEM examinations were performed. Shrinkage and drying tests and mercury intrusion porosimetry were still to be carried out by the time this report was written. Furthermore, detailed investigations will be planned based on the preliminary results partly presented and discussed in this paper.

EXPERIMENTAL

Two groups of sample specimens were investigated within the study, Group A and Group B. The first group (Group A) was produced in order to study the effects of process parameters. The second group (Group B), which was previously produced and had side cracks, was investigated in order to study the effects of drying shrinkage. Mixture design of composite ingredients for both samples in groups A and B was made up of 89,5 % cement, 3,5 % cellulose fibers, 2 % PVA, 3 % silica fume and 2 % sepiolite. The use of silica fume is usually intended to reduce the capillary porosity by filling the micro pores within the paste. Sepiolite, on the other hand, aids the process by reducing the backwater solid concentration by acting as a flocculant, and improving layer bonding by providing links between layers due to its microfibers.

The dimensions of the fiber-cement sheets are 92 cm x 250 cm with 5 ¼ corrugations. This type of corrugation is common in Europe and is sometimes known as the 5 corrugation. The corrugation height is 51 mm and the distance between two crests is 177 mm. The dry thickness of the sheets are approximately 6 mm. Samples used in all tests and analysis were taken from the mid of the sheet for Group A and from the edge of the sheet for Group B. This edge is where the side cracks were observed. Figures 1 and 2 illustrate the locations of the test samples on the sheet.
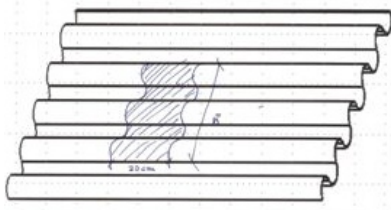
Figure 1: Location of Group A samples
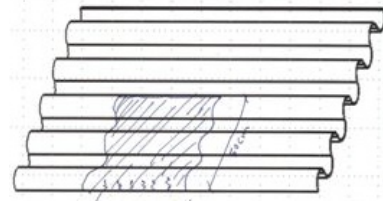
Figure 2: Location of Group B samples

Group A sample specimens were produced in the plant under controlled process parameters with variations that are assumed to be ways of controlling the physical and mechanical properties. The production parameters such as slurry temperature, felt speed, line pressure, and the number of layers of the sheet are ways to control the water and interlayer void ratio and subsequently the percentage of the pores. Therefore, in a controlled environment all these factors are varied to minimum and maximum extremes while maintaining a stable production in a standard 3-Vat Hatschek machine. Variations in vacuum were necessary to control the stable process of production. In Table 1 codes and the process parameters of sample specimens are given. All other process parameters and raw materials were kept at a constant while the above mentioned factors were varied in turns. Each specimen group consists of 4 sample sheets taken from production after the change made has stabilized and all other factors were equal. All these sheets were produced in the same machine with the same raw materials on the same day. Temperature and humidity were all controlled. The sheets were corrugated and were dried at 50 °C in a drying tunnel after which they were immersed in water and stretch wrapped as per the standard procedures of the plant. The first 28 days of curing was done in a controlled environment of constant temperature of 25-30 °C inside the plant.

The second group (Group B) sample sheets were previously produced under standard process parameters. However, these Group B sheets have gone through a cycle of dry heat under the sun without a protective cover stretch film in conditions of 35-40 °C and relative humidity of 20-30 % in a windy location under the sun. Some of these sheets have had side cracks as a result of the fast drying of the sheet in the pallet.

November 15-18, 2006 São Paulo – Brazil

Table 1 – Codes and process parameters.

Code	Control Parametre	Temperature of Slurry (°C)	Felt Speed (m/min)	Line Pressure (kg/cm)	Number of Layers	Vacuum	
						1	2
A2	Low Slurry Temperature	31	44,7	33	7	300	140
A3	Normal conditions	41	44,7	33	7	300	140
A4	Low felt speed	42	32,0	33	7	300	140
A5	High felt speed	45	50,0	33	7	300	140
A6	High line pressure	45	45,0	36	7	300	140
A7	Low line pressure	45	45,0	19	7	300	140
A10	High number of layers	45	44,8	33	9	200	220
A11	Normal number of layers	45	44,8	33	7	200	220
B	Standard	45	44,8	33	7	300	140

Bending

For the bending test, for each sample specimen a total of 16 samples, measuring 30 mm × 150 mm × 6 mm, were prepared from 4 different sheets. Samples were cut with a diamond saw (with water) longitudinally from the edges of the corrugations. Samples were first immersed in water for 24 hours before testing. The flexural strength was determined by 4-point bending test (Figure 3) conducted on wet samples using the universal testing machine (Instron, model 5569) with a capacity of 1 kN. Deflections were monitored by a Solartron LVDT gauging probe with a 5 mm measuring stroke. The displacement speed was 1,5 mm/min.

Figure 3: 4-point bending.

Figure 4: Delamination after bending.

Layer Bonding (pull off)

Samples measuring approximately 30 mm × 50 mm × 6 mm were cut from the broken samples of bending test for testing the delamination of the layers (Figures 5 and 6). 10-15 samples were prepared for each sample specimen discarding the samples already delaminated (those extending along lengthwise) after bending (Figure 4). Samples were bonded to the steel plates using epoxy adhesive and tensile load was applied with the abovementioned universal testing machine.

Figure 5: Pull off.

Figure 6: Delamination after pull off.

Water Absorption

Before the water absorption, samples were dried in the oven at 60 °C until they reached to a constant weight. It took the samples 8 hours to reach the stable dry weight. Afterwards, all the samples were completely immersed in tap water with a temperature of 20 °C in the laboratory. The water level above the samples was kept constant and free water circulation was maintained around and under the samples. During the water absorption phase, all samples were periodically taken out, excess water was eliminated and the samples were weighed. This procedure was repeated continuously until a stable weight was reached. The rate of absorption and maximum water absorption at saturation were then calculated as a percentage of the dry weight (mass).

SEM

Polished sections were examined using a LEO 440 stereoscan model scanning electron microscope (SEM) and images were taken at backscattered electron (BE) mode. Elemental analyses were made by using Oxford Link Isis X-ray ED analysis system.

Porosity

Adsorption/desorption isotherms, specific surface area (BET) and pore size distribution of sample specimens were measured by nitrogen adsorption/desorption at LN2 temperature (~77 K) using a Micromeritics ASAP 2010 analyzer. The detection range of pore diameter with nitrogen desorption was from 17 Å to 3000 Å. According to IUPAC pore size classification, pore diameter smaller than 20 Å is categorized as micro, ranged between 20 Å and 500 Å categorized as meso, and larger than 500 Å is categorized as macro pores (IUPAC, 1985). The total porosity of the hydrated cement paste is made up of C-S-H gel pores (micro pores) and capillary pores (meso and macro pores) apart from the entrapped interlayer air voids. For best evaluation, the pore size distribution should be characterized over the whole range which requires both nitrogen adsorption and mercury intrusion complementary techniques. Therefore, mercury intrusion porosimetry will be applied at a later time for completion of the meso and macro pore (and/or void) sizes of above 300 nm. With mercury intrusion technique pore diameter range between 3 nm and 360 μm can be measured.

RESULTS AND DISCUSSION

Bending

The averages of 4-point bending test results are summarised in Table 2. Among all samples Sample A2 showed the highest modulus of rupture (MOR) while the lowest is observed for Sample B. Effect of drying shrinkage on flexural strength can be best evaluated by comparison of samples A3 and B, since both samples were produced under the standard process parameters, despite the small difference in slurry temperature which might be neglected. Between these two samples approximately 20-25 % reduction in flexural strength is observed. The difference of approximately 25 %, can be attributed partly to the location from where the samples were taken and partly to the difference in slurry temperature. The slurry temperature of 10 degrees between samples A2 and A3 showed a considerable effect in MOR and E-modulus. However, this difference is not as much effective on MOR as the 4 degrees difference between samples A3 and B. Therefore, it is concluded that drying shrinkage, compared to slurry temperature, is a more important factor for MOR. In Figures 7 and 8 stress-deflection curves are shown for samples A3 and B. Measured fracture toughness (specific energy) was significantly lower for sample B indicating the weakness as a result of high drying shrinkage from the edges which might be leading to side cracking. The difference in MOR values of A10 and A11 is the smallest indicating that the number of layers has a minor effect. Line pressure (samples A6 and A7) and felt speed (samples A4 and A5) did not appear to be important parameters in this case.

Table 2 – Flexural strength results.

	Maximum Flexure load (N)	Flexure stress at Maximum Flexure load MOR (MPa)	Elastic Modulus (Segment 0,5 MPa - 3 MPa) E (MPa)	Flexure extension at Maximum Flexure load (mm)	Specific Energy (KJ/m²)
A2	98,77	15,13	8153,10	15,91	7,71
A3	113,03	13,42	5153,72	15,26	7,65
A4	117,43	13,34	6376,31	14,86	7,50
A5	116,84	14,77	7493,93	11,05	5,87
A6	109,40	14,45	7064,11	14,19	7,12
A7	110,15	12,82	6046,84	13,20	6,29
A10	111,36	12,78	6286,95	15,39	7,33
A11	91,23	12,30	6486,05	14,53	6,04
B	86,22	10,63	7389,70	11,49	4,27
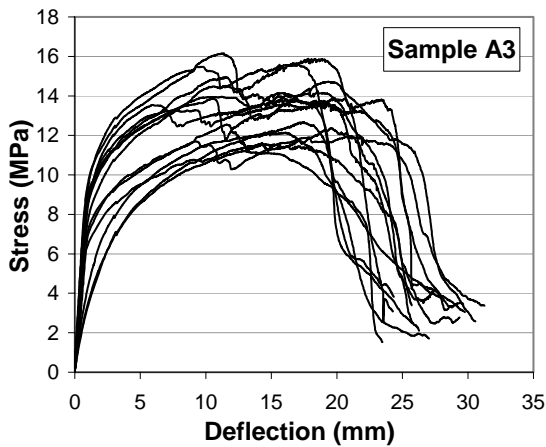
Figure 7: Bending stress behaviour of sample A3.
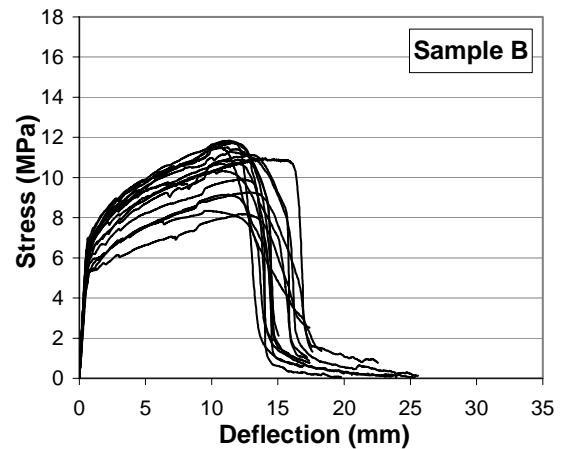
Figure 8: Bending stress behaviour of sample B.

Layer Bonding (pull off)

A2 and A11 are the two specimens which did not show any delamination in any of the 16 samples after bending test. All other samples, more or less, showed delamination between layers. Delamination occurred with highest number of samples for specimens A4 (Figure 4), A6 and A7 after bending. In the evaluation of the pull off test results, the samples in which rupture did not occur 100 % within the specimen, were disregarded in the calculation of the mean.

Table 3 – Layer bonding results.

	Thickness (mm)	Load (N)	Strength (MPa)
A2	5,28	2696,10	1,70
A3	5,96	1363,90	0,87
A4	6,12	996,95	0,63
A5	5,81	1430,23	0,92
A6	5,70	1143,98	0,73
A7	6,05	1293,91	0,82
A10	6,07	1659,87	1,07
A11	5,62	1307,57	0,83
B	5,79	1339,14	0,83
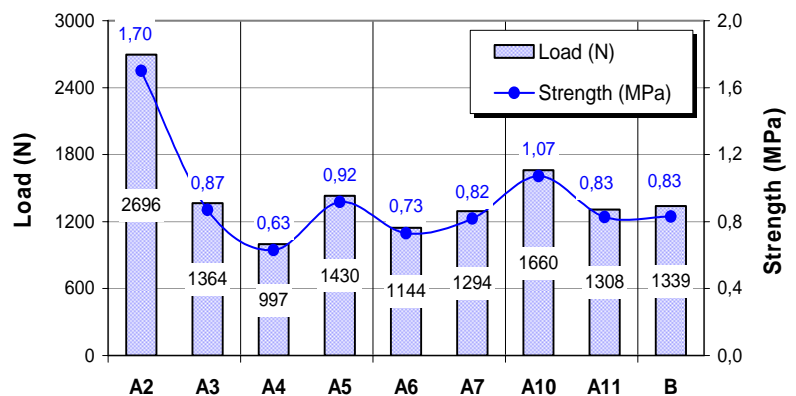
Figure 9: Layer bonding.

Averages of interlayer bonding results obtained from the pull off test are presented in Table 3 and Figure 9. The results clearly indicate that slurry temperature, A2 and A3, is the most effective parameter on delamination. The high layer bond strength of sample A2 can be correlated with its sheet thickness being the thinnest which means it is a relatively dense material. Likewise, the lowest bond strength of sample A4 can be correlated with its thickness being the thickest for the same number of layers as for all other samples except for A10, and reveals a relatively porous material. Low slurry temperature slows down the hydration process and prevents moisture loss. Since the matrix is kept moist for a longer time, C-S-H production increases. Accordingly, the capillary porosity decreases which results in increased strength gain. The next effective parameter on delamination seems to be the felt speed. Higher the felt speed, stronger is the bonding (A4 and A5). This might be related to the higher water ratio remained after vacuums which were able to suck lower

November 15-18, 2006 São Paulo – Brazil

amounts in a shorter time. Sufficient water of hydration is required for better layer bonding. The difference in bonding strength of samples A6 (with high line pressure) and A7 (with low line pressure) is negligible. However, this small difference can be explained by the reduction in water as a result of higher pressure and the resulting dryness leading to a weak bond between layers. The bond strength of sample B, on the other hand, appeared to be in an average level.

SEM

In SEM examinations, weak layer bonds were clearly observed in most samples, except for sample A2, which demonstrated a significantly good adhesion between layers (Figures 10 and 11). In addition, sample A10 also showed better layer bonding characteristics compared to the others. Despite some difficulties, on some samples, all seven layers of the lamina could be counted through air gaps extending longitudinally between the layers. Pull off test results confirm the SEM observations on layer delamination. In general, fiber distribution in the lamina seems to be quite homogenous in most samples (Figure 12). However, the orientation was not random, but in a more regular way. They were mainly arranged parallel to layer intersections and oriented in two directions, the majority being in one. Some large interconnected pores in the cement matrix forming a network at the surface zone were occasionally observed in samples A3, A4, A5 and A10 (Figure 13). High porosity at the surface zone, increasing the permeability, accelerates the drying rate which may cause cracking behaviour.
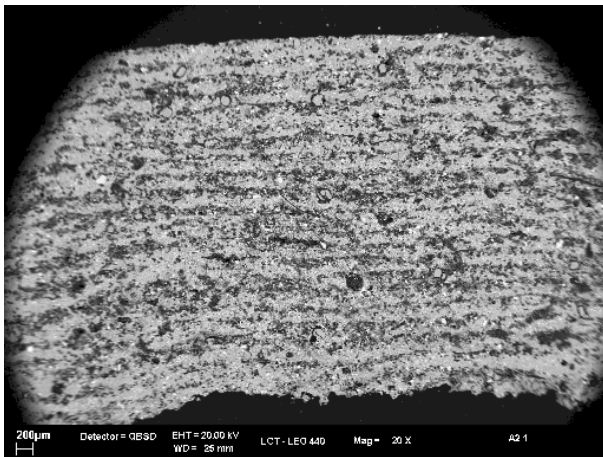
Figure 10: Sample A2, example for good layer bond.
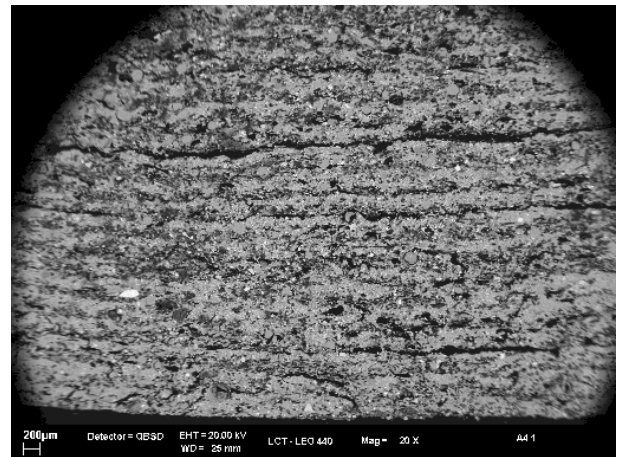
Figure 11: Sample A4, example for weak layer bond.

Regarding the fiber-cement bond, as it is known, evaporation of water in the cellulose fibers during drying causes the fibers to shrink resulting in a weak bond and increased porosity. This was clearly seen particularly for the fibers close to the surface (Figure 14). PVA fibers (round with a smooth surface), on the other hand, demonstrated very strong bonding with cement paste.

Being a pozzolanic material, silica fume (micro silica) reacts with $CaOH_2$ and fill the micro pores of the cement paste with CSH. Thus the use in composites is generally intended to reduce the porosity and consequently increase the strength and decrease the permeability. Silica fume is extremely fine and the particle size of a high-quality is typically around 0,1 µm in diameter (Taylor, 1997). Silica fume particles detected as small globules in the composites were measured up to 30,23 µm on SEM images (Figure 15). In this case, large silica fume particles may not be quite as beneficial as expected. Therefore, the effectiveness of silica fume is questionable and needs further investigation.

November 15-18, 2006 São Paulo – Brazil
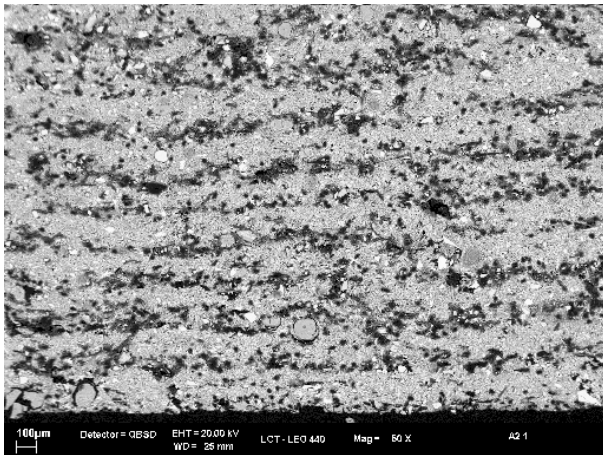
Figure 12: Fiber dispersion.
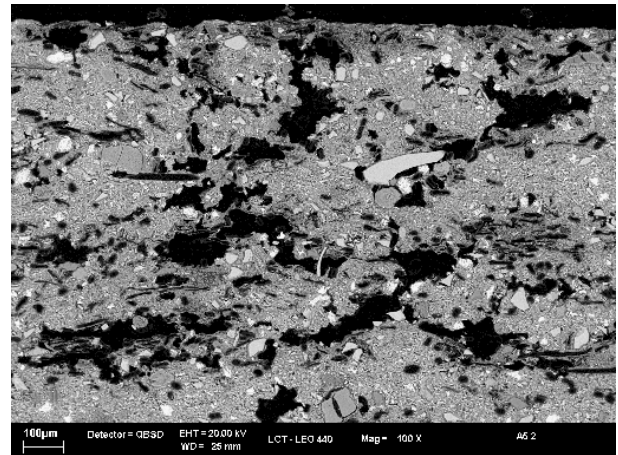
Figure 13: High porosity at the surface zone.
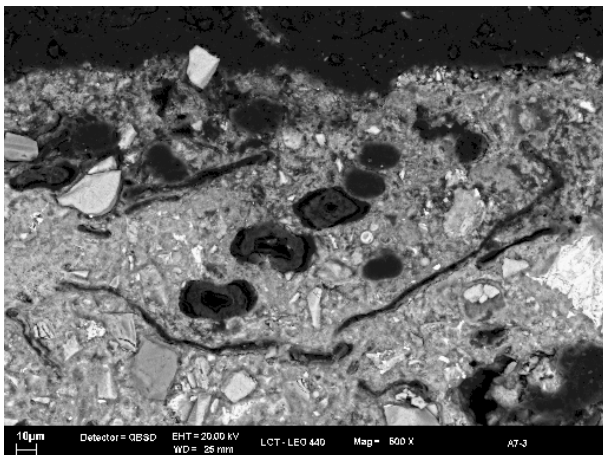
Figure 14: Cellulose fiber shrinkage and PVA bond.
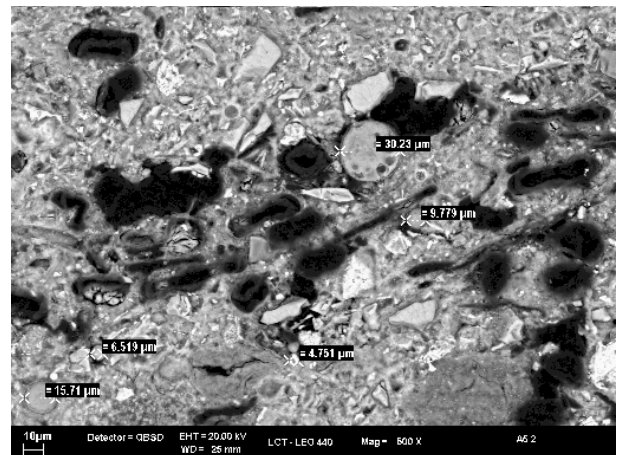
Figure 15: Silica fume in varying sizes.

Porosity

Porosity analysis with nitrogen adsorption/desorption were made for samples A2, A3, A4, A5 and B. The derived results, in general, give information about the C-S-H gel porosity of the test samples. A more detailed discussion can only be made after the complementary mercury intrusion porosimetry measurements.

The summary of obtained data, including BET specific surface area, is given in Table 4 for comparative purposes. Nitrogen desorption data indicates that differences in specific process parameters (i.e. between A2 and A3, A4 and A5) has no significant effect on BET specific surface area. Very small difference in BET results was observed between sample A3 and sample B, which were both produced under the standard process conditions. Indeed, some higher BET specific surface area was expected from sample B as a result of drying shrinkage, indicating some higher porosity at the edges of the sheet. The average pore size of all samples falls into the category of capillary pores. The highest average pore size within the detection range was observed for sample B.

Table 4: Summary of nitrogen desorption data.

	BET (m²/g)	Micropore Area (m²/g)	BJH Desorption Average Pore Diameter (Å)
A2	24,52	1,3323	59,0168
A3	26,11	3,7894	69,0431
A4	64,36	5,5668	48,7880
A5	64,56	6,1285	48,9753
B	26,91	5,3863	92,2600

The microporous structure of samples A2, A3, A4, A5 and B characterized by nitrogen sorption isotherm (relative pressure) is shown in Figure 16. The results show quite large hysteresis between adsorption and desorption isotherms for all samples measured. The difference between the adsorption and desorption curves starting from 1,0 (P/P0) indicates that the material has probably macro pores besides the meso and micro pores. There is insignificant difference between samples A2 and A3, A4 and A5. The sudden drop in the desorption isotherm of sample A4 and A5 is most likely to be generated by the irreversible capillary condensation of the nitrogen in the mesopores which is characteristic of either ink-bottle shaped pores (type H2) or voids between close-packed spherical particles. The hysteresis loops of A2, A3 and B fall into the category of H3 type. H3 loops are found with slit shaped pores. Hysteresis loops types H2 and H3 exhibit a character of type IV physisorption isotherm according to IUPAC classification (IUPAC, 1985).
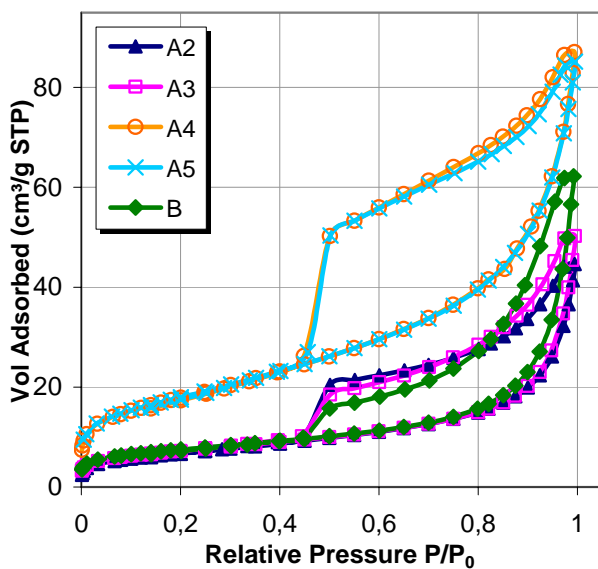
Figure 16: Sorption isotherm curves.
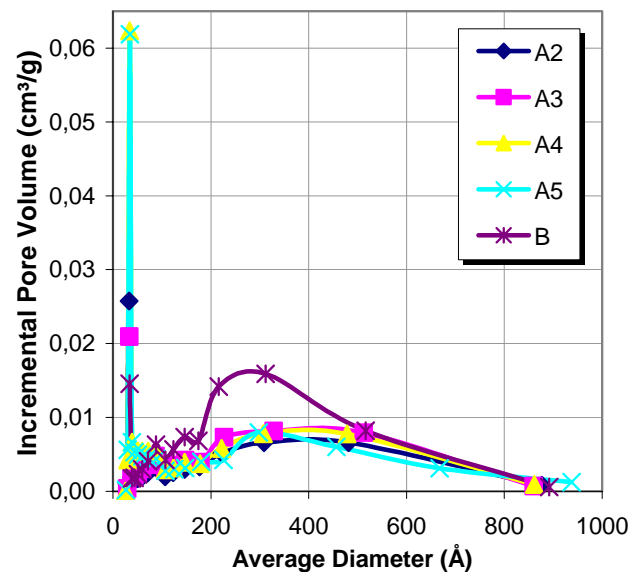
Figure 17: Incremental pore volume plot.

Figure 17 displays incremental pore volume plot. There is a high accumulation of 30 Å pores for samples A4 and A5 whereas this is significantly lower for other samples. Sample B exhibits a relatively higher (meso) porosity within the range 200 – 400 Å. This increase in porosity may be explained by the relatively higher rates of evaporation leading to drying shrinkage and resulting in cracks at the edges of the fiber-cement sheets.

Water Absorption

The absorption rates of sample specimens are displayed in Figure 18 and the maximum water absorption (water absorption saturation) amount by weight (%) in Figure 19.   The water absorption rate decreases considerably for all samples after the first 6 hours. A10 and A11 were the two samples which demonstrated the highest rates of water absorption and the highest saturation amounts. Number of layers increases the number of gaps between layers, therefore a sheet made with more number of layers has more porosity in the gaps between the layers. This result was expected for A10. A11 and A3 have the same process parameter conditions except for the vacuum levels. The difference in water absorption results of A11 and A3 can be explained with their strength. MOR of A3 was somewhat higher than that of A11. The higher the strength, lower is the porosity and thus permeability. The relationship between water absorption and strength is, in general, in good agreement.

The maximum water absorption of sample A2 is significantly lower than all other samples. The relatively low absorption, and in turn, low porosity of A2 can be correlated with its high strength. Lower slurry temperature could result in a slower cement reaction during the formation of the sheet. This could result in ample time for intralayer diffusion to occur therefore less number of pores. Effects of slurry temperature (A2 and A3) and line pressure (A6 and A7) on water absorption seem to be relatively higher than other two parameters. Line pressure has a major effect on porosity. In fact, more line pressure aids in a better adhesion of the layers reducing the gap between them. But, the layer bonding test result of A6 is somehow lower and did not seem to match this postulate. Lower felt speed produces a sheet which has more porosity. We were expecting the opposite result thinking that slower felt speed means more vacuum (when vacuum levels are equal) and less water left in the sheet before the reaction begins, therefore less unreacted water which would evaporate and leave pores behind. Apparently this was not the case. The reason for more porosity in slower felt speed could be explained by less drainage in the sieve because of less centrifugal force and therefore a looser layer formation as explained by Dr. I. I. Berney (Berney, 1968 and 1969).
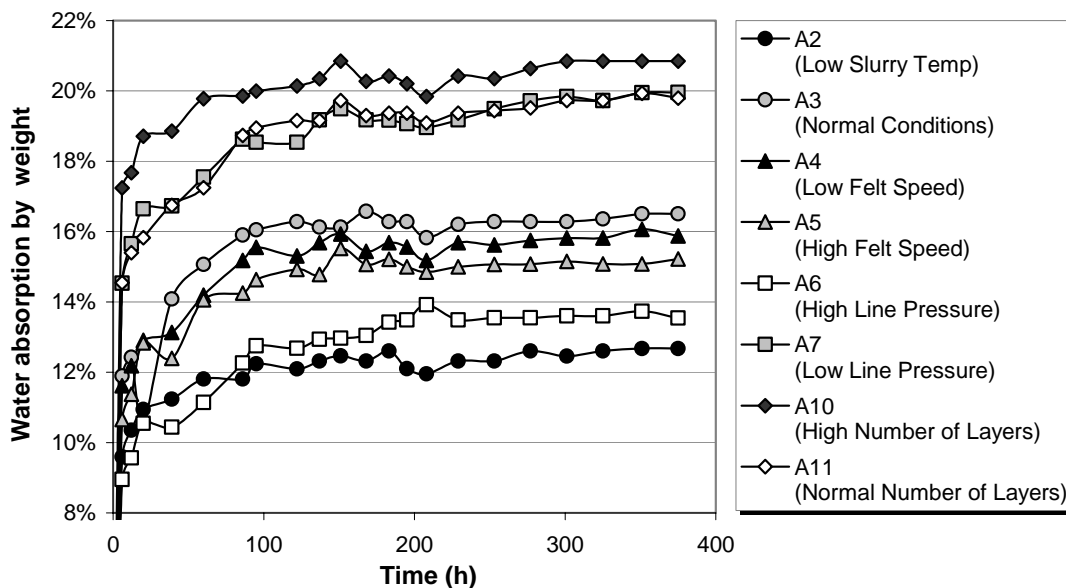
Figure 18: Water absorption rates of samples in Group A.
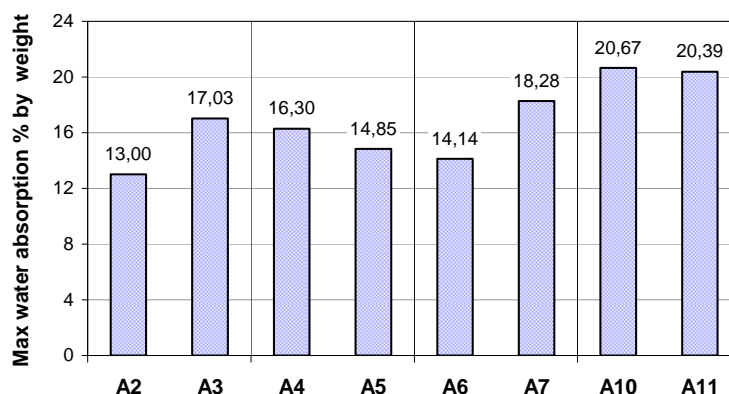
Figure 19: Maximum water absorption amounts of samples in Group A.

CONCLUSION

The overall results (Table 5) show a good correlation between mechanical and physical tests (particularly flexural strength and water absorption) and the microstructural characteristics of all samples tested. The most effective process parameter was found to be the slurry temperature. Remarkable difference was observed between the samples A2 and A3. Sample A2 (low slurry temperature) demonstrated superior mechanical and physical properties among all others. The least effective process parameter was found to be the number of layers. No significant difference was observed between the samples A10 and A11. Hence, the mechanical and physical properties were relatively lower than the other samples, except for the layer bonding strength. Line pressure has considerable effect on flexural strength and water absorption. Sample A6 (high line pressure) was the second best composite in terms of MOR and water absorption properties. For some reason, the layer bonding strength was found to be low. Felt speed was regarded as an important factor to work further. There were apparent differences between mechanical and physical performances of samples A4 and A5. Sample A5 (high felt speed) gave similar results as that of sample A6 (high line pressure). Sample B, as it was expected, showed to be the weakest in flexural strength. Nitrogen adsorption measurements indicated relatively higher meso pores for sample B implying higher drying shrinkage at the edges. SEM examinations, on the other hand, revealed delamination problem in some samples.

Preliminary results will be confirmed with complementary tests and analysis. Further investigations will focus on the process parameters which proved to be the most effective in material properties.

Table 5: Brief summary of test results

Test samples (Process parameter)	MOR (MPa)	Layer Bonding (MPa)	Water Absorption % (by weight)	N2 Adsorption / Desorption (17 Å – 3000 Å)
A2 / A3 (Slurry Temperature)	15,13 / 13,42	1,70 / 0,87	13,00 / 17,03	Evenly distributed
A4 / **A5** (Felt speed)	13,34 / 14,77	0,63 / 0,92	16,03 / 14,85	Evenly distributed
A6 / A7 (Line pressure)	14,45 / 12,82	0,73 / 0,82	14,14 / 18,28	-
A10 / A11 (Number of layers)	12,78 / 12,30	1,07 / 0,83	20,67 / 20,39	-
B (subjected to non-ideal curing conditions)	10,63	0,83	-	Increased mesopores

ACKNOWLEDGEMENTS

REFERENCES

Berney, I.I. 1968. "Asbestos-cement manufacturing technology". Parts I – V.

Berney, I.I. 1969. "Asbestos-cement manufacturing technology". Parts VI – XI.

International Union of Pure and Applied Chemistry (IUPAC). 1985. "Reporting physisorption data for gas/solid systems with special reference to the determination of surface area and porosity". Pure & Appl. Chem., (57) 603-619.

Taylor, H.F.W. 1997. "Cement Chemistry". 2. Edition. Thomas Telford Services Ltd.